Intensity and phase measurements of nondiffracting beams generated with a magneto-optic spatial light modulator

Jeffrey A. Davis, E. Carcole, and Don M. Cottrell

Nondiffracting beams are of interest for optical metrology applications because the size of the beam does not change as the beam propagates. However, accuracy can be increased if the diameter of the beam is smaller. One technique for accomplishing this is to use the dark axial intensity profile associated with a higher-order nondiffracting Bessel function beam. We generate these higher-order Bessel function beams with a programmable spatial light modulator. We study the intensity patterns and the phase dependence of these nondiffracting beams. In addition, we examine interference effects caused by recording these patterns onto a binary spatial light modulator.

Key words: Nondiffracting beams, Bessel function beams, spatial light modulators, diffractive optical elements.

1. Introduction

New kinds of optical lenses[1–4] have been proposed that form zero intensity along the optical axis. For these lenses the size of the dark focal spot can be smaller than the size of the corresponding bright focal spot leading to increased positional accuracy. These lens patterns are also of interest because the output pattern consists of phase singularities.[5] However, the spot size increases rapidly away from the focus point of the lens.

In related research Durnin *et al.*[6] have shown that an optical beam with a Bessel function electric-field profile can propagate without diffraction. Such optical beams can have applications in such areas as optical alignment, surveying, or optical interconnections. However, the positional accuracy of the beam is ultimately limited by the width of the beam. Higher-order nondiffracting Bessel function beams with zero axial intensity have also been reported.[7] The size of the dark spot for the first-order Bessel function beam was smaller than the size of the corresponding bright spot from the zero-order Bessel function beam.

In this research we form diffractive optical elements that create these higher-order nondiffracting beams with a programmable spatial light modulator (SLM). Consequently the size of the beam and the direction of the propagation axis of the beam can be varied,[8] allowing dynamic scanning of the beam. We also examine two new aspects of this problem. First, we study the phase dependence of these nondiffracting beams by superimposing them onto a constant dc background. In addition, we show the consequences of writing the patterns onto a binary phase-only medium. Experimental results are reported in which the patterns are written onto the magneto-optic spatial light modulator[9] (MOSLM).

2. Theory

Beams that approximate this Bessel function nondiffracting behavior can be created with a hologram.[7,10] To create higher-order nondiffracting beams, an angular phase shift is introduced onto the hologram transmission function[7] as

$$T_n(r, \theta) = \exp(in\theta)\exp(-i2\pi r/r_0), \tag{1}$$

where θ and r are coordinates in the hologram plane, r_0 is an adjustable scale factor, and n is an integer.

The electric field that is formed at a distance z away from the plane of the hologram is obtained from Fresnel diffraction theory[7,10] with polar coordinates as

The authors are with the Department of Physics, San Diego State University, San Diego, California 92182. E. Carcole's permanent address is the Departament de Fisica, Universitat Autonoma de Barcelona, Bellaterra 08193, Spain.

Received 7 April 1995; revised manuscript received 2 October 1995.

0003-6935/96/040593-06$06.00/0

$$E(\rho, \phi, z) = \frac{\exp(ikz)}{ikz} \exp\left(\frac{ik\rho^2}{2z}\right) \int_0^R \int_0^{2\pi} T_n(r, \theta) \times \exp\left(\frac{ikr^2}{2z}\right) \exp\left[\frac{-ikr\rho \cos(\theta - \phi)}{z}\right] 2\pi r dr d\theta. \tag{2}$$

Here ρ and ϕ are coordinates in the observation plane, and R is the radius of the hologram. To perform the angular portion of the integral, we change the variables as $-\pi/2 + \alpha = \theta - \phi$. Substituting Eq. (1) for the transmission function, performing the angular integral, and using the integral definition of Bessel functions, we obtain

$$E(\rho, \phi, z) = \frac{\exp(ikz)}{ikz} \exp\left(\frac{ik\rho^2}{2z}\right) \exp\left[in\left(\phi - \frac{\pi}{2}\right)\right] \times \int_0^R \exp\left(\frac{ikr^2}{2z}\right) \exp\left(\frac{-i2\pi r}{r_0}\right) J_n\left(\frac{kr\rho}{z}\right) r dr. \tag{3}$$

In previous work[7,10] this integral was evaluated with the stationary phase method and was evaluated at point $r_c = z\lambda/r_0$. We are particularly interested in the phase associated with this integral. The electric field is given by

$$E(\rho, \phi, z) = C(r_0)\sqrt{z} J_n\left(\frac{2\pi\rho}{r_0}\right) \exp(i\gamma_n). \tag{4}$$

Here the constant $C(r_0) = \lambda^{2.5}/(i^{2.5} r_0)$, and the phase γ_n is given by

$$\gamma_n = kz + n\left(\phi - \frac{\pi}{2}\right)] + \frac{\pi\lambda z}{{r_0}^2} + \frac{k\rho^2}{2z}. \tag{5}$$

This output represents an nth-order Bessel function profile $J_n(\rho)$. The amplitude of the electric field[7,10] increases as $\sqrt{z}$ to a maximum value at a distance of roughly $L = Rr_0/\lambda$ and then sharply decreases. The beam width remains constant over a distance of approximately L and has a value (for the zero-order Bessel function beam) of $W_0 = 0.766 r_0$.

There are four terms in the expression for the phase γ_n. Although these terms are not detectable in intensity, we examine them with an interference technique. The first term is the usual phase associated with a traveling plane wave. The second term shows an azimuthal phase variation, and the number of cycles increases with the order n of the Bessel function. The third term shows an additional longitudinal phase variation. Finally the fourth term represents a quadratic phase front. As we explain below, the last term is not detected, and we assume that it remains as a consequence of the approximations made in the stationary phase method.

The patterns of Eq. (1) can be encoded[8] onto a SLM by writing $r^2 = (i^2 + j^2)(\Delta^2)$, where i and j are integers identifying each pixel and Δ is the pixel spacing. In this case, $r_0 = q\Delta$, where q is an adjustable parameter, N is the number of pixels in the SLM, and the size of the hologram can be written as $R = N\Delta/2$. With these parameters the expression for nondiffracting propagation distance L can be written as

$$L = \frac{qN\Delta^2}{2\lambda}. \tag{6}$$

The beam width W_0 (for the zero-order Bessel function) can be written as

$$W_0 = 0.766 q\Delta. \tag{7}$$

When the value for q is changed, both the beam diameter and the nondiffracting propagation distance are changed.

Figure 1(a) shows the hologram that encodes the zero-order Bessel function J_0 for parameter $q = 4$. When written onto the MOSLM with a pixel size of $\Delta = 75$ μm and $N = 128$, this hologram results in a nondiffracting beam with a width of 230 μm and a maximum propagation distance of $L = 2.28$ m. The patterns (again for $q = 4$) associated with the J_1 and J_2 Bessel functions (for $n = 1$ and $n = 2$) are shown in Figs. 1(b) and 1(c), respectively, and are characterized by spiral arms. As the order of the Bessel function increases, the number of spiral arms also increases.

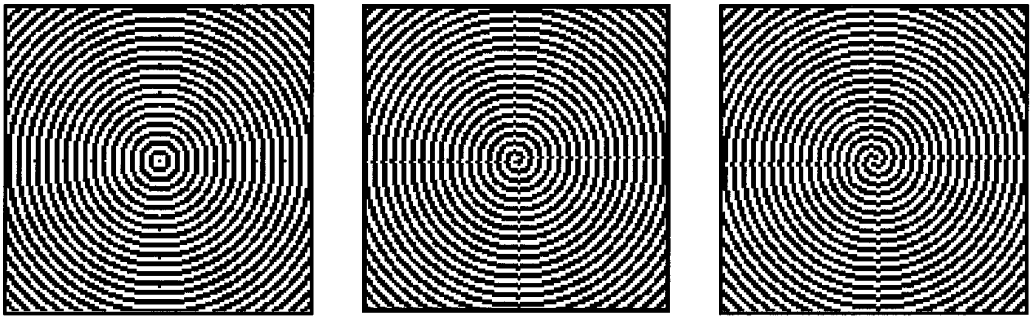

(a) (b) (c)

Fig. 1. Patterns written onto the MOSLM that form (a) the J_0 Bessel function beam, (b) the J_1 Bessel function beam, and (c) J_2 Bessel function beam.

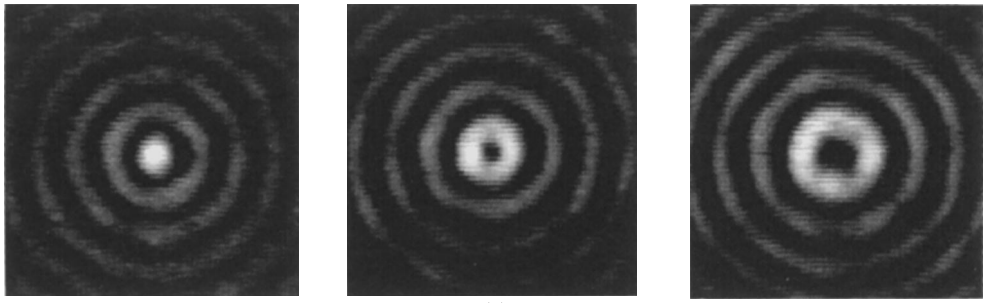

Fig. 2. Output intensities measured at a distance of 1.55 m from the MOSLM showing (a) the J_0 Bessel function beam, (b) the J_1 Bessel function beam, and (c) the J_2 Bessel function beam.

When a linear phase shift is multiplied by this pattern, much of this detail is obscured.[8]

3. Experimental Results

These masks were written onto a MOSLM manufactured by Semetex Corporation operating in the binary phase-only mode.[11] The MOSLM was illuminated with collimated light from a He–Ne laser, and the output beam was recorded with a CCD camera with a pixel size of 12 μm connected to the Macintosh computer through a ComputerEyes interface system.

We have experimentally generated the first eight Bessel function beams. Experimental intensities are shown in Fig. 2 for the J_0, J_1, and J_2 Bessel function beams at a distance of 1.55 m with the corresponding patterns from Fig. 1. The area of the figure is approximately 1.5 mm $\times$ 1.5 mm. It is critical that the aberrations from the SLM be corrected to generate these output beams. Otherwise the electric-field profile is strongly distorted. A simple technique for evaluating these aberrations has been described elsewhere[12] and was used to obtain these results.

As the order of the Bessel function increases, the diameter of the dark spot increases as expected. The diameter of the dark spot for the J_1 beam is clearly smaller than the spot size for the J_0 beam in agreement with theory. The main lobes of the J_1 Bessel function are separated by 204 $\pm$ 36 μm (where the error is caused by the pixel size of the camera) in good agreement with the theoretical value of 170 μm. The diameter of the dark spot for the J_1 beam in Fig. 2(b) is 72 $\pm$ 12 μm. This is much smaller than the size of the J_0 Bessel function beam shown in Fig. 2(a) in agreement with theory.

The higher-order Bessel function beams are also nondiffracting. Figure 3 shows the J_1 Bessel function beam measured at distances of 0.9, 1.55, and 2.20 m, and the size of the beam remains constant. Similar results were obtained for all the higher-order Bessel function beams.

As with the zero-order nondiffracting beam,[8] we have demonstrated that we can translate and rotate the propagation axes of these nondiffracting beams by modifying the generating patterns written onto the MOSLM.

4. Phase Dependence of Bessel Function Beams

We can examine the phase dependence predicted by Eq. (5) by adding an additional dc intensity beam and examining the resulting interference between the nondiffracting beam and the dc beam. This can be experimentally implemented by adjusting the output polarizer on the MOSLM that allows a dc component to be transmitted.[11] The dc electric field is a traveling plane wave and is written as

$$E_{\mathrm{dc}} \exp(ikz). \tag{8}$$

The total light intensity $I(z)$ then varies as a function of propagation distance caused by interference effects between the Bessel function beam and the

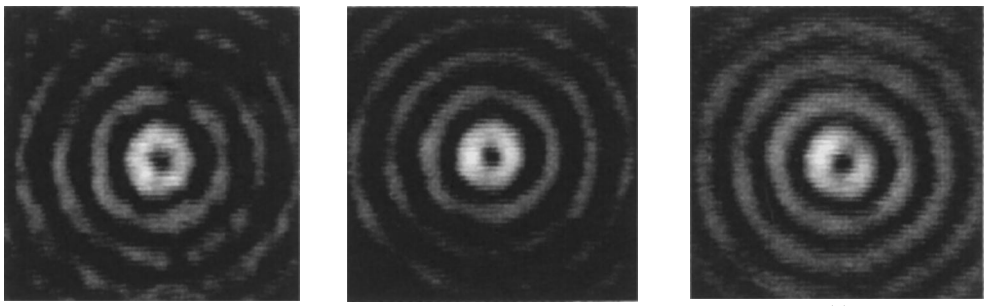

Fig. 3. Output intensity for the J_1 Bessel function beam at distances of (a) 0.9 m, (b) 1.55 m, (c) 2.20 m.

uniform dc beam as

$$I(z) = E_{\mathrm{dc}}{}^2 + E_{Jn}{}^2(\rho) + 2E_{\mathrm{dc}}E_{Jn}(\rho) \times \cos\left[n\left(\phi - \frac{\pi}{2}\right) - \frac{\pi\lambda z}{r_0{}^2} + \frac{k\rho^2}{2z}\right], \quad (9)$$

where E_{dc} is the dc electric field and $E_{Jn}(\rho)$ is the amplitude of the J_n Bessel function electric field defined by

$$E_{Jn}(\rho) = C(r_0)\sqrt{z}J_n\left(\frac{2\pi\rho}{r_0}\right). \quad (10)$$

The interference term in Eq. (9) allows us to examine the phase dependence for the Bessel function beam. Initially we examined the intensity pattern near the origin (where $\rho \approx 0$) and neglected the third phase term. At a given distance z the intensity pattern goes through n maxima as the angular variable ϕ varies from 0 to 2π. However, because of the second phase term, the orientation of this intensity pattern appears to rotate as the distance z is changed. The period D, defined as the distance z between two indistinguishable intensity patterns, is obtained from Eq. (9) by

$$D = \frac{2r_0{}^2}{\lambda}. \quad (11)$$

For our experimental parameters this distance $D = 28.4$ cm. Figure 4(a) shows the interference pattern for the J_1 beam at a distance of $4D = 1.128$ m. The intensity pattern for the J_1 Bessel function beam shows a single maximum as the angular variable ϕ varies from 0 to 2π as expected. Note that the intensity pattern reverses for each successively larger ring caused by the π phase shift between successive rings for the J_1 Bessel function. For example, in Fig. 4(a), the first and third rings are open at the top whereas the second, fourth, and sixth rings are open at the bottom. Figures 4(b) and 4(c) show the intensity patterns at spacings of $z = D/4 = 7.1$ cm, and, as expected, the patterns rotate by $\pi/2$ rad. Experiments examining higher-order Bessel function beams displayed the same characteristics. Note that the distance D between successive identical intensity patterns does not depend on the order n of the Bessel function.

As mentioned above, we see no evidence of the radial phase-dependent term. If this quadratic phase term were present in Fig. 4(a), the open area of each successive ring would be rotated by an additional angle that would increase quadratically with radius relative to the radius of the previous ring. At the edges of the figure where $\rho = 0.75$ mm this radial phase term would have a value of $k\rho^2/2z \approx 2.5$ rad. This is not observed. Therefore we assume that this radial phase term is an error that arises from the approximations in applying the method of stationary phase. Consequently the actual phase shift given in Eq. (5) should not have a radial phase dependence.

5. Effects of Binarizing the Phase Pattern

In showing the propagation of the Bessel functions, we did not show the beam at closer distances than $z = 90$ cm. At distances shorter than this value the intensity pattern changed as a function of z, alternately forming a well-defined spot and then a hole pattern. In this section we show that this effect is caused by the binarization of the pattern written onto the SLM. Depending on the recording medium that is used,[7,8,10] the pattern of Eq. (1) is encoded as a binary phase-only pattern or as a binary amplitude-only pattern. In these cases some interesting effects appear.

The binarized pattern corresponding to Eq. (1) can be expanded in a Fourier series as

$$\sum_{p=-\infty}^{\infty} a_p T_n{}^p(r, \theta) = \sum_{p=-\infty}^{\infty} a_p \exp(inp\theta)\exp(-i2\pi pr/r_0), \quad (12)$$

where the strength of each term in the Fourier series is denoted by the coefficient a_p.

Because the patterns shown in Fig. 1 are square-wave gratings, the values for the first few coefficients are given (assuming a binary phase-only pattern) by

$$a_0 = 0, \quad a_{\pm 1} = 2/\pi, \quad a_{\pm 2} = 0, \quad a_{\pm 3} = 2/3\pi. \quad (13)$$

Note that these nonzero coefficients can be written

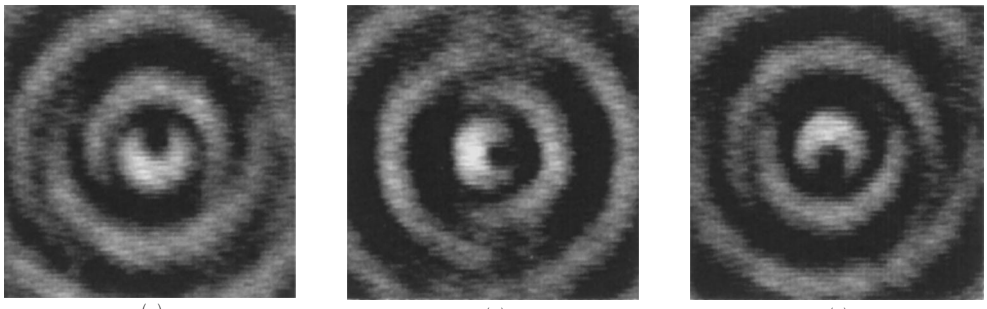

(a) (b) (c)

Fig. 4. Interference patterns formed between the dc beam and the J_1 Bessel function beam at distances of (a) 1.128 m, (b) 1.199 m, (c) 1.270 m.

as $2/p\pi$. Following the analysis of Eqs. (2)–(5), we can represent the output as a series of Bessel-function-type outputs as

$$\sum_{p=-\infty}^{\infty} a_p C(r_0/p)\sqrt{z}\,\exp(i\gamma_{np})J_{np}\left(\frac{2\pi p\rho}{r_0}\right) = K\sum_{p=-\infty}^{\infty}\sqrt{z}\,\exp(i\gamma_{np})J_n\left(\frac{2\pi p\rho}{r_0}\right). \quad (14)$$

Here $K = a_p C(r_0/p)$ is a constant that is independent of p. Therefore each order in Eq. (14) has the same strength. The phase shifts γ_{np} are now given by

$$\gamma_{np}(\rho, z, \phi, r_0) = np\left(\phi - \frac{\pi}{2}\right) - \frac{\pi\lambda p^2 z}{{r_0}^2}. \quad (15)$$

The output consists of a superposition of several Bessel function beams, each with an effective size that is proportional to the radius r_0/p and with an effective transmission distance of L/p. The contribution from the $p = 1$ component has the largest beam profile and will propagate over the longest distance of L. The higher orders, corresponding to the $p = 3$ and $p = 5$ orders, produce beams with narrower profiles that propagate over shorter distances. Figure 5 shows the schematic behavior of these beams. The largest $p = 1$ beam travels a distance corresponding to L. The higher-order beams corresponding to $p = 3$ and $p = 5$ are smaller and travel a shorter distance as indicated in the figure. The negative orders correspond to virtual nondiffracting beams and are not observed.

In a region where multiple beams coexist, interference effects occur between the various higher-order Bessel function beams. In the patterns shown in Fig. 3, no such interference effects were seen because the patterns were measured at distances greater than $L/3$ where the intensities of the higher-order beams are negligible. However, at shorter distances the resulting pattern has different characteristics caused by these interference effects. For the region between $L/3$ and $L/5$ we have interference between the wider J_n and the narrower J_{3n} beams. In the region between $L/5$ and $L/7$ there is interference between the J_n, J_{3n}, and J_{5n} beams where again the diameters of these beams are different. This difference in diameters affects the radial contrast in the interference pattern. The contrast in the interference pattern should not change with propagation distance z. However, more exact numerical evaluations of the Fresnel diffraction integral[7] show some intensity oscillations with propagation distance. Consequently the contrast ratio changes slightly with distance.

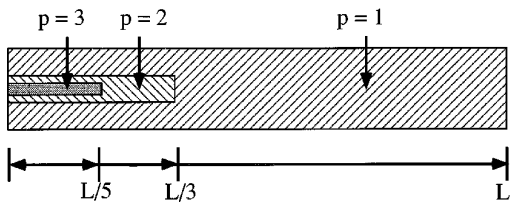

Fig. 5. Formation of higher-order Bessel function beams by the binary patterns shown in Fig. 1.

These effects were examined experimentally in the region between L and $L/3$ for the zero-order Bessel function beam where $q = 4$ and where $p = 1$ and $p = 3$ contributions interfere. Following the treatment in Section 4, we can write the intensity (for $n = 0$) as

$$I(z) = (a_0 E_{J01})^2 + (a_3 E_{J03})^2 + 2a_0 a_3 E_{J01} E_{J03}\cos\left(\frac{8\pi\lambda z}{{r_0}^2}\right). \quad (16)$$

When the two Bessel function electric fields are in phase, the intensity is strongest at the origin because of the interference between two strongly peaked functions with different widths. When the two electric fields are out of phase, the destructive interference at the origin leaves a doughnut-shaped pattern. The intensity pattern oscillates as a function of distance z and repeats at distances of D' defined as

$$D' = \frac{4{r_0}^2}{\lambda}. \quad (17)$$

Experimental examination of these interference effects is complicated by the aberrations from the SLM. As mentioned above, these aberrations can be compensated[12] by multiplying the transmission function $T(r, \theta)$ in Eq. (1) by the complex conjugate $A^*(r, \theta)$ of the aberrating function.

However, when the new function $A(r, \theta)T(r, \theta)$ is binarized as in Eq. (12), the effective binarized aperture function becomes

$$\sum_{p=-\infty}^{\infty} a_p A^p(r, \theta) T_n{}^p(r, \theta). \quad (18)$$

Consequently, when the pattern is multiplied by the complex conjugate of the aberrating pattern $A^*(r, \theta)$, the aberrations are corrected for only the $p = 1$ term. The higher-order terms cannot be simultaneously corrected. Fortunately we found a MOSLM with no aberrations for this experiment.

For our experimental parameters, distance $D' = 3.55$ cm. Experimental results are shown in Fig. 6. Figure 6(a), taken at a distance of $z = 60.45$ cm, shows destructive interference between the wider $p = 1$ beam and the narrower $p = 3$ beam that results in the doughnut-shaped pattern. Figure 6(b) is taken at a distance of $z = 62.22$ cm and shows constructive interference. Here the width of the beam appears smaller because the intensity was much stronger and we had to adjust the sensitivity of the camera to avoid saturation. Otherwise the width of the beam would have been the same as in Fig. 6(a). We again see destructive interference at a distance of $z = 64.00$ cm as shown in Fig. 6(c). The measured distance between successive maxima or minima is 3.55 cm, in

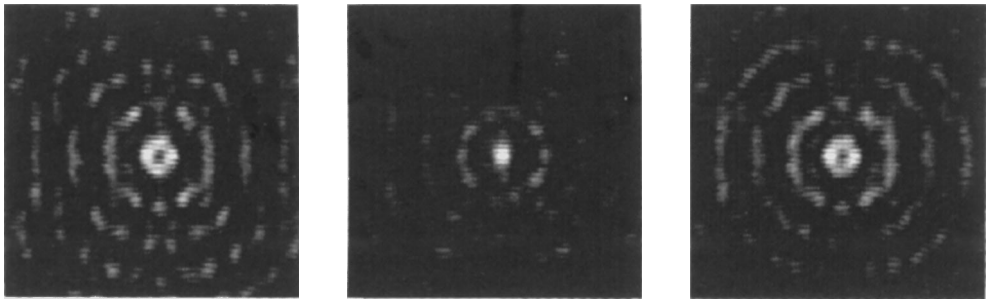

(a) (b) (c)

Fig. 6. Interference patterns formed between $p = 1$ and $p = 3$ harmonics of the binarized pattern for the J_0 Bessel function beam at distances of (a) 0.6045 m, (b) 0.6222 m, (c) 0.6400 m.

excellent agreement with theory. As mentioned above, the contrast changes slightly as the propagation distance changes and we have chosen a distance with excellent contrast to demonstrate this interference. As the distance increases further than approximately $z = 90$ cm, all interference effects disappear because the $p = 3$ beam does not propagate beyond this point.

6. Conclusions

This research shows that higher-order Bessel function nondiffracting beams can be generated with programmable SLM's. It is critical that aberrations on the SLM be corrected to obtain these results. The width of the dark spot formed with a first-order Bessel function beam is smaller than the corresponding width of the bright spot for the zero-order Bessel function and may be useful for such applications as surveying in which the width of the beam is an important parameter. We also confirm the phase dependence of these Bessel function beams by examining the interference with a dc beam. However, we find that the quadratic phase term is not seen experimentally. We suspect that this term arises because of the approximations in performing the Fresnel integral with the method of stationary phase. Finally we examine the effects of binarizing the pattern that generates these Bessel function beams and show that additional higher-order beams are generated with different widths and different propagation distances. In regions where these beams overlap, the resulting interference modifies the shape of the nondiffracting beam. However, it can still be used for alignment purposes. At sufficiently long distances the beam behaves as expected. By varying the pattern written onto the SLM, we can vary the nature of the nondiffracting beam as well as the propagation axis at the frame rate of the SLM.

One of us (E. Carcole) acknowledges grant BE94/1-58 Annex-1 from Generalitat de Catalunya, Catalunya, Spain.

References

1. S. B. Vinas, Z. Jaroszewicz, A. Kolodziejczyk, and M. Sypek, "Zone plates with black focal spots," Appl. Opt. **31,** 192–198 (1992).
2. J. Ojeda-Castaneda, P. Andres, and M. Martinez-Corral, "Zero axial intensity by annular screens with angular variation," Appl. Opt. **31,** 4600–4602 (1992).
3. J. Ojeda-Castaneda and G. Ramirez, "Zone plates for zero axial intensity," Opt. Lett. **18,** 87–89 (1993).
4. Z. Jaroszewicz and A. Kolodziejczyk, "Zone plates performing generalized Hankel transforms and their metrological applications," Opt. Commun. **102,** 391–396 (1993).
5. N. R. Heckenberg, R. McDuff, C. P. Smith, and A. G. White, "Generating of optical phase singularities by computer-generated holograms," Opt. Lett. **17,** 221–223 (1992).
6. J. Durnin, J. J. Miceli, Jr., and J. H. Eberly, "Diffraction-free beams," Phys. Rev. Lett. **58,** 1499–1501 (1987).
7. A. Vasara, J. Turunen, and A. T. Friberg, "Realization of general nondiffracting beams with computer-generated holograms," J. Opt. Soc. Am. A **6,** 1748–1754 (1989).
8. J. A. Davis, J. Guertin, and D. M. Cottrell, "Diffraction-free beams generated with programmable spatial light modulators," Appl. Opt. **32,** 6368–6370 (1993).
9. W. E. Ross, D. Psaltis, and R. H. Anderson, "Two-dimensional magneto-optic spatial light modulator for signal processing," Opt. Eng. **22,** 485–490 (1983).
10. J. Turunen, A. Vasara, and A. T. Friberg, "Holographic generation of diffraction-free beams," Appl. Opt. **27,** 3959–3962 (1988).
11. D. Psaltis, E. G. Paek, and S. S. Venkatesh, "Optical image correlation with a binary spatial light modulator," Opt. Eng. **23,** 698–704 (1984).
12. E. Carcole, J. A. Davis, and D. M. Cottrell, "Astigmatic phase correction for the magneto-optic spatial light modulator," Appl. Opt. **34,** 5118–5120 (1995).